Enhanced Nanofluidization by Alternating Electric Fields

Daniel Lepek
New Jersey Center for Engineered Particulates, New Jersey Institute of Technology, Newark, NJ 07102

Jose Manuel Valverde
Faculty of Physics, University of Seville, Avenida Reina Mercedes s/n, 41012 Seville, Spain

Robert Pfeffer
Dept. of Chemical Engineering, Arizona State University, Tempe, AZ 85281

Rajesh N. Dave
New Jersey Center for Engineered Particulates, New Jersey Institute of Technology, Newark, NJ 07102

DOI 10.1002/aic.11954
Published online August 7, 2009 in Wiley InterScience (www.interscience.wiley.com)

We show experimental results on a proposed technique to enhance the fluidization of nanoparticle beds. This technique consists of the application of an alternating electric field to the nanofluidized bed. Three different field configurations have been tested: co-flow field, cross-flow field, and variable field configurations. Nanoparticle agglomerates are naturally charged by contact and tribo charging mechanisms and therefore are agitated by the action of the externally applied field, which enhance fluidization. According to our observations, the best results are obtained for the variable field configuration. In this configuration, the electric field strength is higher at the bottom of the bed, whereas it is almost negligible at the free surface. Thus, the larger agglomerates, which tend to sink at the bottom of the bed due to stratification, and usually impede uniform fluidization, are strongly agitated. It is thought that the strong agitation of the bigger agglomerates that usually sink to the bottom of the bed contributes to further homogenize the distribution of the gas flow within the bed by destabilizing the development of gas channels close to the gas distributor. On the other hand, the smaller agglomerates at the vicinity of the free surface are just weakly excited. Consequently, fluidization is greatly enhanced, whereas at the same time excessive elutriation is avoided. It is demonstrated that this technique is even suitable to achieve highly expanded fluidization of unsieved nanopowder samples even though the fluidization state returns to be heterogeneous upon the electric field being turned off. © 2009 American Institute of Chemical Engineers *AIChE J,* 56: 54–65, 2010
Keywords: fluidization, nanoparticles, agglomeration, electric fields

Correspondence concerning this article should be addressed to J. M. Valverde at jmillan@us.es
Current Address of Daniel Lepek: The Cooper Union, 41 Cooper Square, New York, NY 10003.

Introduction

The fluidization behavior of solid particles fluidized by dry air at ambient conditions is mainly dependent on two particle properties: size and density. Bubbling fluidization is

the most common behavior found in fluidized beds of coarse grains (typically of size $d_p \gtrsim 100$ μm for particle density $\rho_p \sim 1000$ kg/m^3) as soon as the gas velocity u_g surpasses the minimum fluidization velocity u_{mf} (Geldart B behavior[1]). For intermediate size particles (of particle size between $d_p \sim 20$ μm and $d_p \sim 100$ μm), the van der Waals attractive forces between the particles become comparable to the particle weight and are capable of suppressing bubbles in an interval of gas velocities between u_{mf} and $u_g = u_b > u_{mf}$, where u_b is the gas velocity at bubbling instability (Geldart A behavior[1]). It has been shown that interparticle attractive forces can provide the fluidized bed with an effective elastic modulus that stabilizes it against small disturbances.[2,3] Accordingly, it is observed that interparticle contacts are permanent in this stable expanded state, in which the bed takes the appearance of a weak solid.[4,5] The fluid-like behavior of Geldart A powders is accompanied by the instability to bubbling just when the gas velocity surpasses u_b. Experiments show that enhancing the interparticle force between fluidized coarse grains may effectively shift their fluidization behavior from Geldart B to A. For example, bubbling beds can be stabilized by an incremental addition of a liquid[6] or by fluidizing with highly adsorbing gases that increase the interparticle attraction.[7]

The action of an externally applied electric field has been proven to be effective in stabilizing fluidized beds of semi-insulating Geldart B grains.[8] Generally, it is observed that the field promotes the formation of strings of polarized particles that tend to follow the field lines and fill in the bubbles, thus impeding their growth. Theoretical and experimental studies[8–10] have demonstrated that electric fields of the order of 1 kV/cm are effective in changing the behavior from Geldart B to Geldart A stable fluidization. Semi-insulating grains are required for charge relaxation times to be comparable to the typical time between grain collisions, which allows for charge exchange during collisions, thus preventing the grains from charge accumulation. Furthermore, the increase of surface conductivity allows for higher polarizability of the particles,[10] which enhances interparticle attraction. Surface conductivity is usually enhanced in practice by fluidizing the grains with humidified air.[9] Otherwise, electromechanical effects are seen to be mainly due to the contact charging mechanisms[11] of the insulating dry grains. Then, the most severe effect observed for static and low frequency alternating fields is channeling. Grains build up progressively on the electrodes upon application of the field and the bed finally becomes depleted and diluted.[9]

When the particle size is decreased below ~ 20 μm, natural van der Waals forces between the particles are exceedingly large as compared to particle weight. Consequently, these powders tend to rise as a slug of solids or to form channels through which the fluid escapes rather than being distributed through the bulk (Geldart C behavior[1]). To improve the fluidization uniformity of these fine cohesive powders, the techniques employed are aimed to lessen the effect of the strong adhesion between the particles when compared with particle weight. Usually, external excitations are applied, including vibration or stirring. The addition of flow conditioners, such as silica and titania nanoparticles, which coat the surface of micron sized particles, thus reducing the attractive force between them, makes it possible to drive fine cohesive powders into a nonbubbling quasi-homogeneous fluidization phase. In the nonbubbling regime these coated powders exhibit considerable bed expansion[12–14] characterized by a fluid-like dynamics.[15] This new type of behavior, which was not accounted for in the Geldart's scheme, is ruled by the hydrodynamic interaction between particle agglomerates and the fluidizing gas. Bed expansion is then affected by physical parameters such as agglomerate size and structure[16] and gas viscosity.[17,18]

In contrast with the Geldart C behavior, a number of works have revealed that smooth fluid-like fluidization of some ultrafine powders (submicron particle size) is also observed. Reports of uniform fluidization of submicron particles can be found from the middle 1980s.[19–24] Fluidization of nanoparticles, providing extremely high gas-solid contact efficiency, has become a promising technique for industrial applications. Although some nanoparticles, such as titania nanoparticles, exhibit poor fluidization quality, others, such as silica nanoparticles, can exhibit a fluid-like fluidization behavior, with high bed expansion and absence of visible bubbles in a wide interval of gas velocities.[25] Fluidized nanoparticles are seen to form highly porous agglomerates of size d^{**} on the order of hundred of microns.[26,27] These complex-agglomerates are formed by agglomeration in the fluidized bed of simple-agglomerates of size d^* in the range 1–100 μm that exist previous to fluidization.[28] The agglomeration of simple-agglomerates can be thought as the result of a dynamic equilibrium of the attraction between the simple agglomerates and the hydrodynamic friction from the surrounding gas, that supports the weight of the complex-agglomerates in the gravity field.[29]

Bed expansion of fluidized beds of nanoagglomerates, and consequently the efficiency of gas-solid contact, can be further increased by means of assisted fluidization methods, including external vibration,[26,30] sound wave pulsation,[31] centrifugation,[32] and addition of large magnetic particles that are excited by a variable magnetic field.[33] These techniques promote complex agglomerate agitation, which increases the flow shear on their surface and thus decrease their size, and have been proven to be effective in enhancing the fluidization of presieved samples of silica nanoparticles. Usually, silica nanopowder must be sieved before fluidization tests in order to remove large and hard-to-break agglomerates of sizes up to a few millimeters. In this paper, we investigate the use of alternating electric fields as a method to enhance the dry fluidization of silica nanoparticles. Even though the nanopowder as a whole is electroneutral, insulating dry nanoagglomerates accumulate a significant amount of charge in the fluid-like fluidized bed due to contact charging mechanism.[34] The agglomerate charge absolute value Q^{**}, obtained from manual tracking of the agglomerates subjected to an electrostatic field, was found to be of the order of 10^{-14}C.[34] Experimental observations have shown that fluidized nanoparticle agglomerates excited by an electrostatic field experience an electrophoretic force as a consequence of being naturally charged, which leads to agglomerate electrophoretic deposition on the vessel walls, and subsequent channeling and depletion of the bed.[30,35] In this case, the electrostatic field has a detrimental effect on fluidization. On the other hand, it could be expected that application of an alternating field would serve not just to avoid electrophoretic

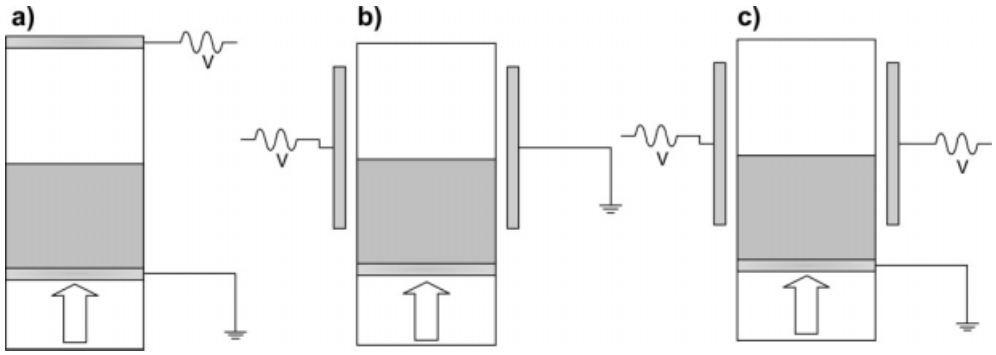

Figure 1. Sketches of the three different setups used in the alternating electric field enhanced fluidization: (a) Co-flow electric field, (b) Cross-flow electric field, (c) Variable electric field. The arrow represents the direction of gas flow.

deposition but also to increase agglomerate agitation, thus enhancing flow shear and bed expansion.[36] Three different alternating electric field configurations have been tested in our work: cross-flow field, co-flow field, and variable field configurations. It will be shown that the variable field configuration, mainly characterized by a strong field at the bottom of the fluidized bed and a weak field close to the free surface, is highly effective in assisting fluidization of even unsieved nanoparticle samples.

Experimental Set-Up

The experiments were performed in a rectangular fluidization cell made of polycarbonate, 4.5 cm in length, 2.5 cm in width, and 21.0 cm in height. Fitted at the bottom of the cell was a rectangular piece of sintered stainless steel (pore size $= 5\ \mu$m). The surface area available for the gas distribution was 11.25 cm^2. Filtered and dried air was chosen as the fluidizing gas for all experiments. The bed height of the fluidized bed was measured using a ruler (marks in mm) taped to the side of the fluidization cell. The gas flow through the fluidized bed was controlled using a MKS flow controller (model 1179A) with a range from 0 to 2000 cm^3/min.

The powder used in all of the experiments was silica Aerosil© R974 ($d_p = 12$ nm, particle density $\rho_p = 2250$ kg/m^3). To reduce any hinderance of fluidization caused by hard large agglomerates, the nanopowder was generally presieved using a 425 μm mesh, although experiments with unsieved silica were also performed for one particular configuration. Previous reports[25,26] show that sieved silica nanopowder exhibits agglomerate particulate fluidization (APF) behavior, which is characterized by a large bed expansion and smooth fluidization. On the contrary, the unsieved nanopowder displays a rather heterogeneous fluidization state characterized by little bed expansion and stable gas channels. It is well known that nanopowder history may have substantial effects on the fluidization behavior of fine cohesive powders[37] because interparticle adhesive forces might be largely increased by stresses applied during previous nanopowder history. Thus, in order to have reproducible results, the memory of the nanopowder should be erased by convenient initialization before any measurement is taken. The initialization procedure followed in our experiments consists of first applying a high gas velocity ($u_g \approx 3$ cm/s). In this state, the nanopowder should have lost memory of its previous history.[37] Additionally, the cell was fixed with a teflon holder to the table of a vertically oriented Tira GmbH vibrator, which enabled us to help fluidized bed initialization when it was needed. Once the bed has reached a stationary state, the gas velocity is decreased to the desired value and bed height is measured. Then the electric field is turned on and the stationary bed height after application of the field is measured as the electric field strength is slowly increased. After each experiment, vibration helped to remove any nanopowder electrostatically deposited on the cell walls.

Three different types of electric field spatial distributions were used in the electric field enhancement fluidization experiments (see Figure 1).

For the horizontal electric field configuration (hereafter referred to as the cross-flow field configuration), two square electrodes (14 cm length) were positioned on either side of the fluidized bed. The distance between the electrodes was held constant at $d = 8.3$ cm. One of the electrodes is grounded and alternating high voltage V is applied to the other from an oscillator-Trek amplifier network. This configuration was used in Ref. 30 to study the effect of an electrostatic field on nanofluidization. From a 3D FEM calculation of the electric field between the electrodes using COMSOL Multiphysics software, it was shown that this configuration produced a rather uniform electric field within the cell, whose strength could be well approximated by $E = V/d$.

For the vertical field configuration (hereafter referred to as the co-flow field configuration), the side electrodes were removed, and instead, a piece of wire mesh (1 mm pore size), with the same rectangular dimensions as the cell cross-section, was suspended by means of a vertical metallic bar at the top of the cell at a distance $d = 8$ cm from the gas distributor plate, which served the function of the other electrode. The voltage distribution and electric field across the electrofluidized bed obtained using COMSOL Multiphysics software by solving the Laplace's equation ($\nabla^2 V(x, y, z) = 0$) indicates that the electric field has a higher strength in the vicinity of both electrodes. Besides of the preferential orientation of the electric field, a relevant difference between the cross-flow and co-flow configurations in our experiments, is that, in the former one, the nanoagglomerates cannot touch the electrodes and thus they remain just naturally charged, whereas, in the latter one, the electrodes are within the

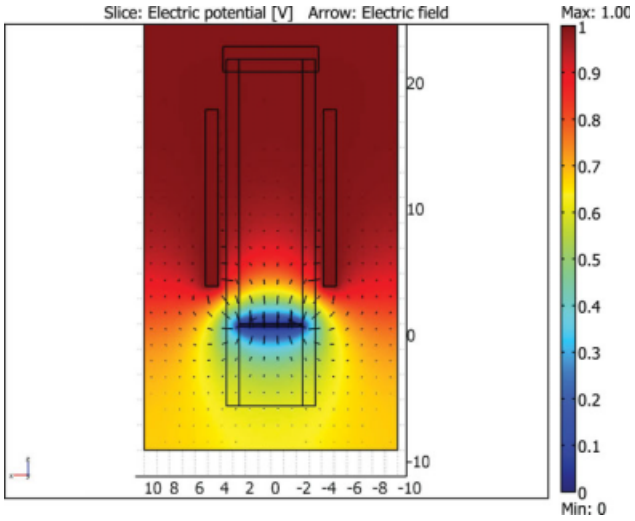

Figure 2. COMSOL simulation results of the voltage and electric field distribution between the electrodes (variable field configuration).

The electrodes and the cell have been drawn to scale, with the distances in cm. Voltage is normalized (the verticals electrodes were set to voltage 1 and the lower electrode was grounded). [Color figure can be viewed in the online issue, which is available at www.interscience.wiley.com.]

fluidized bed, and thus the charge of the particles may change from contact with the electrodes (especially the bottom electrode).

For the third type of electric field configuration (hereafter referred to as the variable field configuration), the two vertical electrodes used for the cross-flow field configuration are in place on either side of the bed and both are held at the same high voltage. The metallic distributor plate at the bottom of the fluidization cell is grounded. Figure 2 shows the distribution of electric potential and field in the mid plane of the cell, which were numerically obtained using 3D FEM COMSOL Multiphysics software by solving the Laplace's equation ($\nabla^2 V(x, y, z) = 0$) with the boundary conditions $V = 1$ at the vertical electrodes and $V = 0$ at the metallic gas distributor plate (the voltage is normalized to its maximum value). It can be seen that the highest potential difference occurs in the region between the vertical electrodes and the distributor plate. Thus, the larger induced electric field is applied in this region. On the other hand, the field between the vertical electrodes is negligible for a bed height of the order of the separation between the electrodes.

The strength of the field along the central vertical axis of the cell in its mid plane is plotted in Figure 3 for the co-flow and variable field configurations. As it was inferred from previous observations, it is seen that the variable field configuration creates a rather nonuniform field within the bed of high intensity in the vicinity of the gas distributor and almost negligible at a height comparable with the distance between the vertical electrodes. The vertical field configuration creates a field of higher intensity in the vicinity of the gas distributor, but also of high strength as the upper electrode is approached.

It is well known that the distribution of agglomerate sizes is quite broad,[27] which gives rise to a marked stratification within the fluidized bed. In the stratified bed, the largest size agglomerates would be at the bottom and the successive layers toward the top would be composed of agglomerates of ever decreasing sizes, with the smallest ones preponderant at the very top. Thus, the interest of the variable field configuration is twofold. By means of a nonuniform electric field of high strength in the vicinity of the gas distributor, the excitation on the larger agglomerates would be enhanced. At the same time, the smaller agglomerates close to the free surface should not be affected by the almost negligible electric field strength in this region, which would be beneficial to avoid excessive elutriation.

The following parameters were chosen as variables for all the experiments: electric field frequency f, electric field strength E_n, and gas velocity u_g. It can be expected that the effect of the electric field would be relevant for field strengths yielding an electric force on the agglomerates F_e^{**} comparable to their weight $W^{**} \simeq 2$ nN, where it has been used $d^{**} = 200$ μm and $\rho^{**} = 50$ kg/m^3 for the agglomerate size and density, respectively.[18,26,27] Thus, alternating field of strengths up to the order $E_n \sim W^{**}/Q^{**} \simeq 2$ kV/cm are applied, which should be sufficient for an observable effect on bed expansion.

We also tested the effect of subjecting the nanopowder bed to an initial corona discharge before fluidization. This was accomplished by placing a metallic pin above the surface of the bed, which was subjected to a high DC voltage in order to allow current to flow from the tip of the pin to the metallic distributor plate, part of which was deposited in the nanopowder.

Results and Discussion

Effect of fluidization cell geometries

In their previous study on the effect of vibration and electrostatic fields on the quality of nanoparticle fluidization,

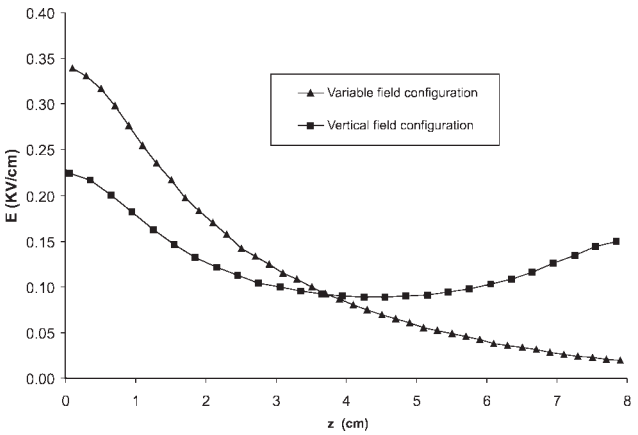

Figure 3. COMSOL simulation results of the electric field strength along the central vertical axis of the bed as a function of the distance to the gas distributor (co-flow and variable field configurations).

The potential difference between the electrodes is set in both cases to 1 kV. In the variable field configuration, the distance between the lower rim of the vertical electrodes and the gas distributor plate (bottom electrode) is 3 cm. In the co-flow configuration, the distance between the top metallic mesh electrode and the gas distributor plate is 8 cm.

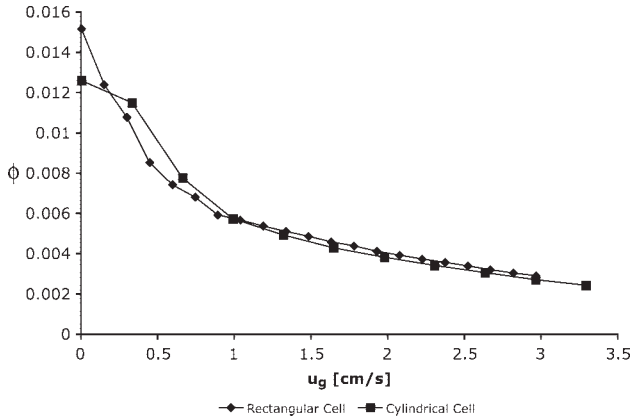

Figure 4. Particle volume fraction (ϕ) as a function of superficial gas velocity in conventional fluidization experiments (in the absence of externally applied electric field) for different cell geometries.

Quintanilla et al.[30] utilized a cylindrical fluidized bed with a diameter of 2.54 cm. Kanyap et al.[35] utilized a rectangular fluidized bed in their study of electrostatic fields. This difference in fluidization cell geometry might have an affect on the quality of fluidization. Thus, a study of the conventional fluidization was performed in our actual rectangular fluidized. The results were directly compared to those reported by Quintanilla et al.[30]

For these experiments, the presieved R974 silica nanopowder was allowed to fluidize conventionally with no external fields. Figure 4 shows the particle volume fraction of the fluidized R974 silica nanopowder as a function of superficial gas velocity u_g. In this plot, as in the following ones, we utilize the particle volume fraction ϕ to measure the expanded state of the fluidized bed, such that $\phi = m/(\rho_p AH)$, where m is the mass of the fluidized nanopowder, ρ_p is the nanopowder material density, A is the area, and H is the height of the fluidized bed. Thus, as the bed expands and the height increases, the particle volume fraction ϕ decreases.

In the conventional fluidization experiment, the particle volume fraction decreases continuously due to the smooth increase in bed expansion as the superficial gas velocity is increased. Further increase of u_g above 3 cm/s gives rise to a significant amount of elutriation. As it can be seen in Figure 4, the fluidization behavior of the R974 silica nanopowder is almost independent of the cell geometry as should be expected from the uniform fluid-like fluidization exhibited by this nanopowder and absence of solid stresses on the particles in this fluid-like regime. Slight deviations in particle volume fraction exist, however, at velocities less than $u_g = 1$ cm/s due to the transitional nature of the nanopowder going from the fluid-like to a solid-like state.[18]

Electrofluidized bed: co-flow field configuration

As it is detailed in the experimental setup section, for the co-flow field configuration experiments, the electrodes were placed inside the fluidized bed. Either electrode could be connected to the high voltage source and used as the live electrode. Two different arrangements were thus used for the experiments. In the first arrangement, the bottom electrode (gas distributor metallic plate) was grounded and the top electrode (wire mesh) was connected to the high voltage source. In the second arrangement, the top electrode was used as live electrode and the bottom electrode was grounded.

A substantial difference in the expansion of the fluidized bed was observed when these different arrangements were used. When the bottom electrode was grounded, moderate bed expansion was observed. However, when the arrangement was reversed, and the top electrode was grounded, much larger bed expansion was observed. Figure 5 shows the relative variation of the particle volume fraction $\Delta\phi/\phi_0$, where $\Delta\phi = \phi - \phi_0$ and ϕ_0 is the initial particle volume fraction for conventional fluidization (i.e., $E_n = 0$), as a function of the nominal electric field strength ($E_n = V/d$) for a fixed gas velocity ($u_g = 0.66$ cm/s) and electric field frequency ($f = 20$ Hz). It can be seen that the larger bed expansion (over 20% larger) can be obtained using the top electrode grounded arrangement. Just slight increments can be obtained for the bottom electrode grounded arrangement (below 10%) but only at very high electric field strengths (results from experiments using different batches were made to confirm this). It can be observed in Figure 5 that in the top grounded electrode arrangement, enhanced bed expansion begins at lower electric field strengths. These experiments were also repeated at a lower gas velocity ($u_g = 0.44$ cm/s). Again, the fluidized bed achieved much greater expansion (almost 20% relative increment) in the top electrode grounded arrangement. A reasonable explanation to why the top electrode grounded arrangement is more effective in obtaining greater bed expansions than the bottom electrode grounded arrangement is that in the former arrangement, more particles are directly exposed to charging at the distributor. In the bottom electrode grounded case, for the particles to become charged, the current needs to pass

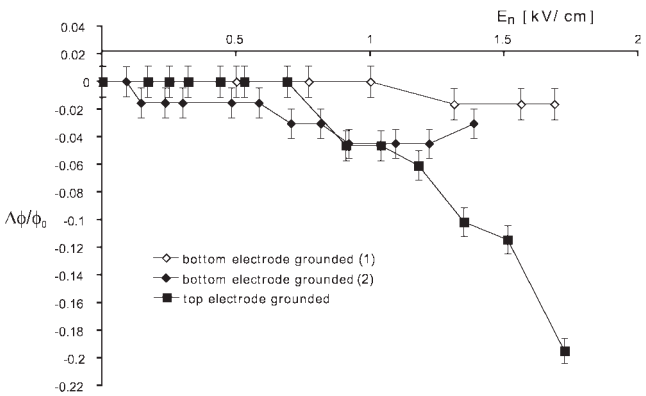

Figure 5. Relative variation of the particle volume fraction ($\Delta\phi/\phi_0$) as a function of nominal electric field strength (E_n) in the co-flow field configuration and for bottom grounded electrode (gas distributor) and top grounded electrode (wire mesh).

Gas velocity $u_g = 0.66$ cm/s and field oscillation frequency (20 Hz) are fixed. Two sets of data for the bottom grounded electrode arrangement are shown corresponding to experiments performed using different batches.

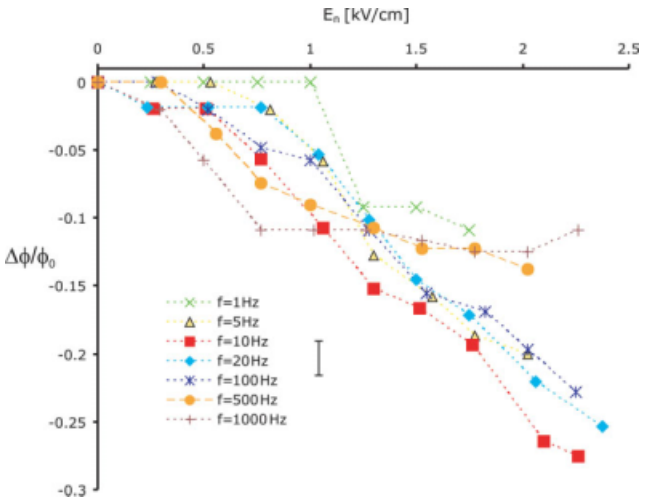

Figure 6. Relative variation of the particle volume fraction ($\Delta\phi/\phi_0$) as a function of nominal electric field strength (E_n) in the co-flow field configuration for different field oscillation frequencies (indicated).

Gas velocity is fixed to $u_g = 0.44$ cm/s. The error bar indicates the experimental indeterminacy. [Color figure can be viewed in the online issue, which is available at www.interscience.wiley.com.]

from the upper electrode, through air, to the surface of the bed. In the top grounded electrode case, the particles in direct contact with the distributor may take charge from it. Higher level of charge will give rise to higher agitation by the applied field and thus to increased fluidization enhancement.

It must be noted however that application of the electric field introduced a certain indeterminacy in the measurements of the bed height. Main sources of this indeterminacy are the blow up of nanopowder that is captured by the upper electrode and the sticking of electrostatically charged nanopowder to the internal walls of the cell that causes an unquantifiable effective lost of mass of the fluidized nanopowder. Because the mass of nanopowder to be fluidized is so small, any lost of mass in fluidization gives rise to a high indeterminacy in the calculation of particle volume fraction. These effects are inherent to the highly polydisperse nature of nanoagglomerate size[18] and charge.[18] This hinders the reproducibility of the results when different batches of nanopowder are used as can be seen in Figure 5, where results are shown obtained from different nanopowder batches for the bottom grounded arrangement. Thus, the results shown in this preliminary research are mostly indicative of a qualitative trend and should be just evaluated as a qualitative comparison of the relative effects of the alternating electric field according to different configurations used.

One of the parameters studied in the vertical field electrofluidized bed experiments was the frequency of the AC sine wave. Previously, it has been observed in the case of vibrofluidized beds that application of a low vibration frequency results in a higher bed expansion and that the effect of frequency becomes less marked at high frequencies.[30] In this work, electrofluidization experiments were performed in which the bed was fluidized at a constant gas velocity and vertical electric fields of different frequencies ($f = 1$, 5, 10, 20, 100, 500, and 1000 Hz) were applied according to the top grounded arrangement. Experimental data for a fixed gas velocity ($u_g = 0.44$ cm/s) are plotted in Figure 6, where it can be seen that the frequency does have a slight effect on the expansion of the fluidized bed. The largest bed expansions ($\Delta\phi/\phi_0 \approx 25\%$) are observed for the frequencies in the intermediate range of $f = 10$–100 Hz. It is seen that less expansion occurs for $f < 10$ Hz and $f > 100$ Hz. Significant electrophoretic deposition of the electrostatically charged agglomerates at the walls and electrodes takes place in the range of small frequencies as seen for DC fields,[30] thus hindering fluidization quality. On the other side, high oscillation frequencies produce very short oscillations of the agglomerates, thus minimizing the enhanced fluidization effect of the field.

The degree to which the fluidized bed has reached an expanded state can affect the further contribution of the electric field to obtaining larger bed expansion. The effect of increasing the electric strength at different constant gas velocities was studied at a fixed frequency. To avoid significant electrophoretic deposition at low field frequencies and lack of effect at high frequencies, a field frequency of 20 Hz was chosen for this study. The data were taken for the top grounded orientation to fully maximize the expansion of the fluidized bed.

Figure 7 shows the relative variation of the particle volume fraction as a function of electric field strength at varying superficial gas velocities. It can be seen that the largest relative bed expansion occurs at lower gas velocities (0.7 cm/s $\leq u_g \leq$ 1 cm/s) when compared with those at higher gas velocities (1.6 cm/s $\leq u_g \leq$ 1.9 cm/s). It can also be observed that the slopes of the expansion curves at each gas velocity are almost the same, implying that the electric field

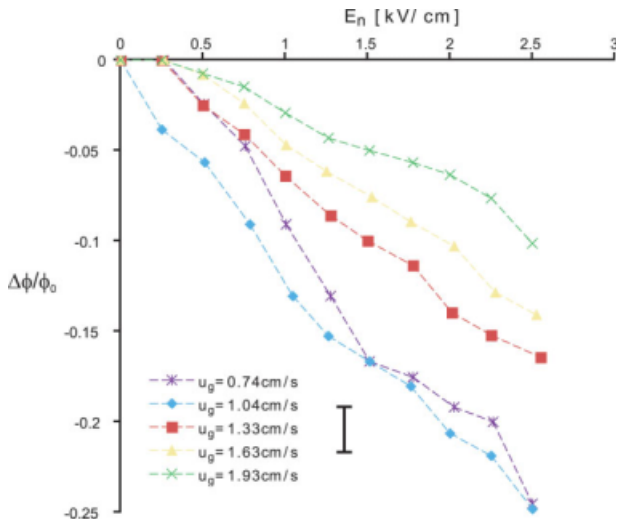

Figure 7. Relative variation of the particle volume fraction ($\Delta\phi/\phi_0$) as a function of nominal electric field strength (E_n) for different gas velocities (indicated) in the co-flow field configuration.

Field oscillation frequency is fixed at 20 Hz. The error bar indicates the experimental indeterminacy. [Color figure can be viewed in the online issue, which is available at www.interscience.wiley.com.]

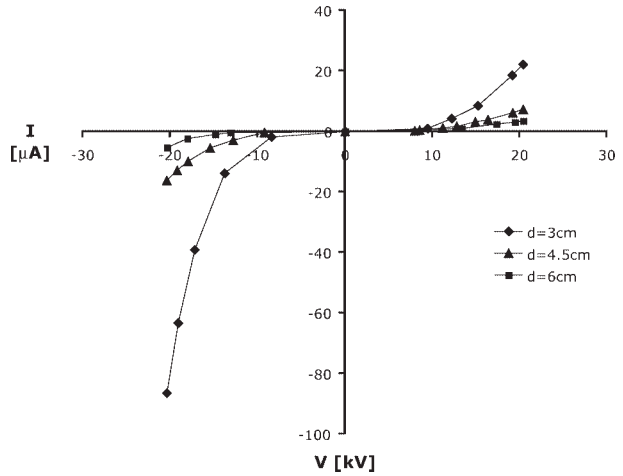

Figure 8. Induced current *I* from the corona discharge as a function of voltage applied *V* at difference distances (indicated) from the tip to the metallic distributor plate.

provides uniform expansion for all gas velocities. This suggests that the electric field is less beneficial when the fluidized bed is in a fully developed fluidized state, almost at the point of elutriation.

The effect of previous artificial charging of the particles was studied in order to compare the fluidization behavior of artificially charged and naturally charged particles. To artificially charge the R974 silica nanopowder before fluidization, we applied a corona discharge by placing a metallic pin above the surface of the bed, which was subjected to a high DC voltage while the distributor plate was grounded. Corona charging of granular layers of insulating millimeter sized particles at the surface of a grounded electrode has been reported in the literature and is used in practice in roll-type electrostatic separators.[38] However, little is known on how the ionic charge is distributed in the material.

Figure 8 shows the induced current I measured in our corona charging experiment as a function of voltage applied V at different distances d between the pin and the distributor. Three major points can be observed from this figure. First, the distance between the pin and the distributor has a large effect on the amount of current that can be transmitted. The largest current observed is at $d = 3$ cm. Distances less than 3 cm were not used so that the bed, when fluidized, would not come in contact with the pin. Second, it can be seen that there is a nonlinear relationship between current and voltage. Third, larger currents can be obtained at negative charging when compared with those used with a positive corona discharge.

To study the effect of corona charging on the fluidization behavior of silica nanoparticles, the following experiments were performed. First, the nanopowder was fluidized conventionally (without corona charging or external field) and allowed to settle. Then, a corona charge was applied to allow the particles to become charged. The nanopowder was precharged using a DC current with a voltage of -12 kV. The nanopowder was then fluidized in the absence of externally applied electric field to see if the previous corona charging itself had any effect on fluidized bed expansion. Finally, the corona charged nanopowder was fluidized in the presence of an externally applied co-flow electric field and using both the bottom grounded and top grounded arrangements. In Figure 9, the particle volume fraction ϕ of the fluidized bed according to these procedures is plotted as a function of superficial gas velocity. It can be seen that the curve with the highest particle volume fractions, which indicates poor fluidization quality, corresponds to the case of the conventional fluidized bed of corona precharged nanopowder. According to visual observations, this is most likely due to an induced strong attraction between the charged particles and the metallic distributor plate. As seen in Figure 9, the hampering effect of corona precharging on fluidization could be, however, compensated by applying a co-flow field only using the top grounded electrode arrangement, whereas the level of expansion could not be recovered by means of the bottom grounded arrangement. This is another indication of the effectiveness of the top grounded arrangement in enhancing bed expansion.

Another parameter varied in precharging the particles was the polarity of the corona discharge. From Figure 8, it was observed that the largest induced current takes place at negative applied voltage. The nanopowder was charged at two different negative corona voltages and one positive voltage to observe how the expansion behavior changes. As it can be seen in Figure 10, the largest expansion for the precharged nanopowder fluidized with no external fields occurs in the case of the positive corona charging. This is in good agreement with Figure 8 because the smallest induced current was observed at positive voltages. Therefore, the nanopowder is less likely to remain in contact with the distributor plate. For the negative corona charging, it can be seen that the nanopowder fluidizes more difficultly especially at low gas velocities. For the strong negative corona charging ($V =$

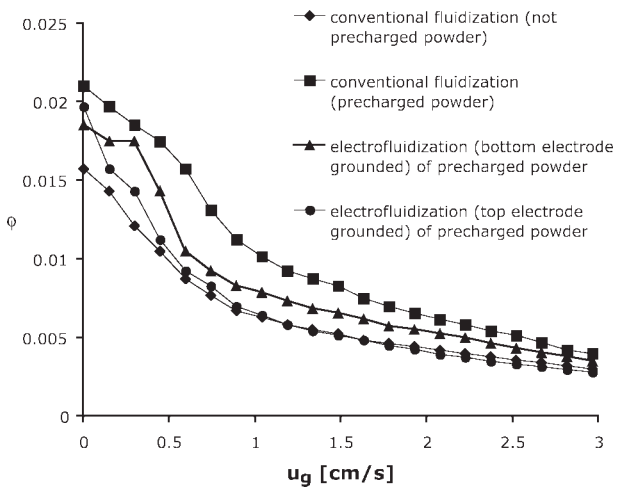

Figure 9. Particle volume fraction ϕ as a function of superficial gas velocity in fluidization of previously precharged nanopowder in the presence of a co-flow electric field for different arrangements as indicated, and in the absence of externally applied electric field (conventional fluidization).

Results from conventional fluidization of not precharged nanopowder (as shown in Figure 4) are shown for comparison.

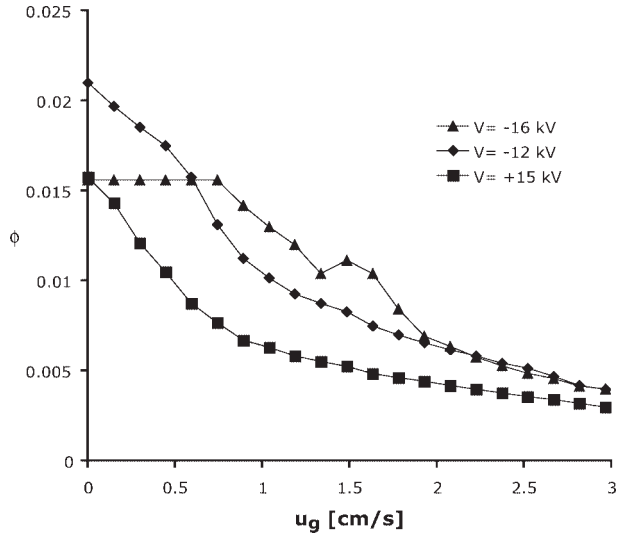

Figure 10. Particle volume fraction ϕ as a function of superficial gas velocity during conventional fluidization (in the absence of externally applied electric field) of the nanopowder previously precharged using corona discharge at different voltage levels as indicated.

-16 kV), the nanopowder is unable to fluidize until almost twice the minimum uniform fluidization velocity in the absence of field is reached ($u_g \approx 2u_{mf} \approx 0.8$ cm/s). The same results inferred from Figure 10 were also observed for the electrofluidized bed in both the top and bottom grounded electrode arrangements. These results imply that corona precharging hinders the expansion of the fluidized bed, unless the externally applied field after corona charging is strong enough to compensate for the particles sticking to the metallic distributor.

An additional effect that must be accounted for is the ionic wind motion originated from DC corona discharges.[39] Ionized air molecules nearby the pin have the same polarity as that of the charged tip. Subsequently, the ionized gas cloud immediately expands due to the repulsive forces. This repulsion of ions creates the so-called corona wind that flows from the tip. Thus, a practical problem with corona charging of fine particles is that nanopowder particles may be airborne and then coat the corona wire, preventing it from being effective.[39] This problem is particularly relevant in our nanofluidized bed. The mean gas velocity associated to the ionic wind can be estimated as $u_g \sim \sqrt{\epsilon/\rho_g}E$, where ϵ and ρ_g are the electric permittivity and density of the gas, respectively, and E is the electric field strength. Using $\epsilon = 8.85 \times 10^{-12}$ F/m, $\rho_g = 1.2$ kg/m^3, and $E = 1$ kV/cm, we obtain $u_g \sim 30$ cm/s, which is more than one order of magnitude larger than the minimum fluidization velocity for our nanopowder. Thus, the corona charging usually sets the nanopowder in turbulent motion. This causes the lost of a significant amount of nanopowder. Also the gas circulation causes compaction of a nanopowder layer against the distributor, which further hampers subsequent fluidization. This compaction effect can be also inferred from Figures 9 and 10, where it is seen that the particle volume fraction ϕ of the previously charged bed in the absence of fluidizing gas flow is above the value of ϕ for the not precharged nanopowder.

Electrofluidized bed: cross-flow field configuration

For the cross-flow field electrofluidized bed experiments, the study of the effect of electric field frequency was performed by observing the fluidized bed expansion as a function of gas velocity at a constant applied electric field strength ($E = 1.25$ kV/cm) for several frequencies. Data of the relative variation of the particle volume fraction $\Delta\phi/\phi_0$ are plotted in Figure 11 showing that that the largest relative expansion obtainable occurs at $f = 20$ Hz as for the co-flow field configuration. As the frequency is increased above 100 Hz, the relative expansion becomes smaller similarly to the results obtained for the co-flow field configuration.

Further cross flow field electrofluidization experiments were performed at $f = 20$ Hz to maximize the enhanced expansion effect of the alternating field. In these experiments, the bed was allowed to expand at a fixed gas velocities. The electric field strength was then slowly increased and the bed height was monitored. Figure 12 shows $\Delta\phi/\phi_0$ as a function of the electric field strength at different gas velocities. It can be seen that the bed expands quite uniformly as the electric field is increased and that, for the higher gas velocities ($u_g > 1.33$ cm/s), larger bed expansions might be obtainable. However, it was observed that the highly expanded bed transited for $E_n \gtrsim 2$ kV/cm into a dilute regime in which the bed surface becomes undistinguishable and a considerable mass of nanopowder was elutriated.

These results are in direct contrast to those obtained from the cross-flow field configuration reported previously using DC electric fields.[30,35] For a DC field, it was shown that fluidized beds of nanoparticles subjected to a electrostatic field in the cross-flow configuration exhibited decreased bed

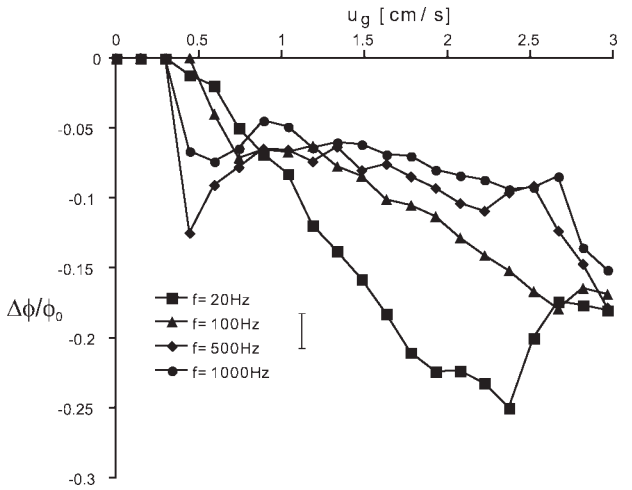

Figure 11. Relative variation of the particle volume fraction ($\Delta\phi/\phi_0$) as a function of superficial gas velocity for different field frequencies (indicated) in the cross-flow field configuration.

Field strength is fixed at 1.25 kV/cm. The error bar indicates the experimental indeterminacy.

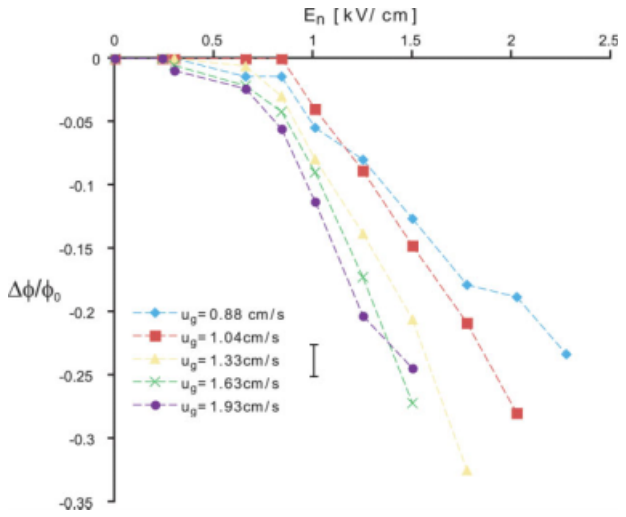

Figure 12. Relative variation of the particle volume fraction ($\Delta\phi/\phi_0$) as a function of nominal electric field strength (E_n) for different gas velocities (indicated) in the cross-flow field configuration.

Field oscillation frequency is fixed at 20 Hz. The error bar indicates the experimental indeterminacy. [Color figure can be viewed in the online issue, which is available at www.interscience.wiley.com.]

expansion as the electric field strength was increased. Contrarily, we show in this work that alternating electric fields enhances the expansion of the fluidized bed as the field strength is increased. A further advantage of the alternating field cross-flow configuration is that the electrodes are not placed inside the fluidization cell, which avoids the negative effects of the electrostatic deposition of the agglomerates on them observed for the co-flow field configuration.

The transition of the bed to a dilute expanded state, and the eventually continuation to the elutriated state, elaborates the point that although the application of a cross-flow electric field can be advantageous to further expanding the fluidized bed, it becomes limited at relatively high gas velocities. In the dilute and elutriated state, the bed surface becomes undistinguishable, and the nanopowder leaves the fluidization cell. The loss of nanopowder can be detrimental to industrial applications at high gas velocities. For that reason, we developed the variable field configuration, in which the highest strength of the field is limited to the bottom of the bed, whereas the field is practically zero at the free surface.

Electrofluidized bed: variable field configuration

Experiments were performed at constant field oscillation frequency ($f = 20$ Hz) for this variable field configuration. At different gas velocities, the voltage applied was increased and the corresponding bed height was measured. Figure 13 displays the relative increase of particle volume fraction as a function of electric field strength at different gas velocities for a distance between the lower rim of the vertical electrodes and the distributor of $d = 3$ cm. The figure shows qualitatively similar results to the ones obtained from previous configurations. A distinct differentiation can be made for the several gas velocities used. The expansion is much more enhanced at lower gas velocities when compared with higher ones. It must be considered that silica R974 is a special kind of nanopowder that can be well fluidized even without the aid of an electric field at high velocities. Thus, it is reasonable that the electric field fluidization enhancement is more effective at lower gas velocities.

One of the parameters that can be varied for the variable field configuration is the distance of the vertical electrodes to the distributor plate. In the first set of experiments, the distance between the lower rim of the vertical electrodes and the distributor plate was $d = 5$ cm but the relative increase of expansion observed ($\approx$3.75%) was almost a complete order of magnitude smaller than the increase measured for the other configurations and any noticeable expansion did not occur until the field reached a strength of approximately $E_n \approx 2$ kV/cm. The vertical electrodes were then lowered to $d = 3$ cm, for which expansion enhancement is already considerable at $E_n \approx 0.8$ kV/cm. It is expected that bed expansion will be further enhanced if the vertical electrodes are further lowered.

An interesting observation for this configuration is the strong agitation of the agglomerates in the region of high strength field, which can be inferred for the observed slight vortex motion of the nanopowder near the gas distributor plate. This indicates that the strong field close to the gas distributor helps to vigorously agitate the larger agglomerates that sink to the bottom of the bed and usually hamper additional bed expansion. The agitation of these large agglomerates further destabilizes the development of gas channels close to the gas distributor. An additional advantage of this variable field configuration is that the amount of elutriation is visibly reduced when compared with enhanced fluidization experiments using cross-flow and co-flow field

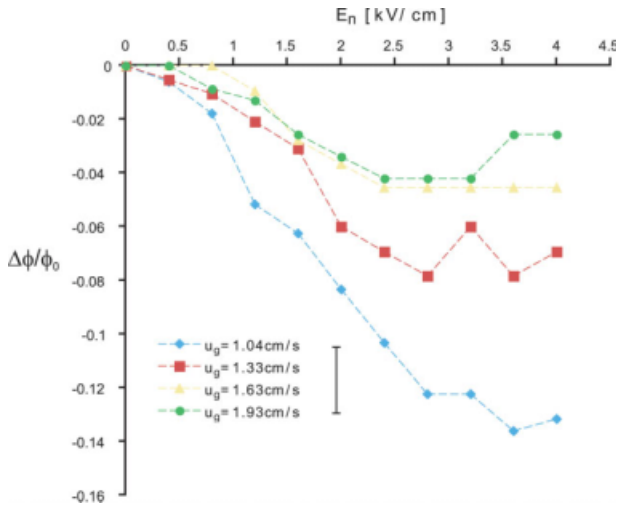

Figure 13. Relative variation of the particle volume fraction ($\Delta\phi/\phi_0$) as a function of nominal electric field strength (E_n) for varying gas velocities (indicated) in the variable field configuration.

The distance between the lower rim of the vertical electrodes and the metallic gas distributor is $d = 3$ cm. [Color figure can be viewed in the online issue, which is available at www.interscience.wiley.com.]

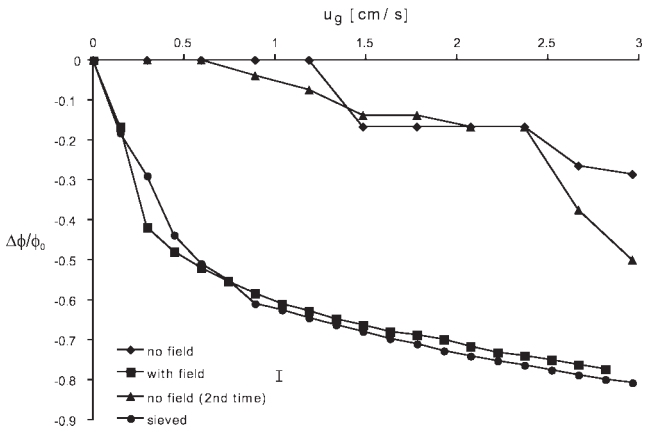

Figure 14. Relative variation of the particle volume fraction ($\Delta\phi/\phi_0$) as a function of gas velocity for unsieved R974 silica with and without electric field applied (variable field configuration).

Nominal field strength ($E_n = V/d$) is fixed at 4 kV/cm. Data from conventional fluidization of sieved silica (without electric field applied) is shown for comparison.

configurations. Even at the higher voltage differences, the bed surface is seen to remain clearly distinguishable and there is little nanopowder loss due to the minimized elutriation.

It is noticeable that at very high nominal electric field strengths, gas bubbles close to the distributor are developed. These bubbles do curtail further expansion as seen in Figure 13, where it is observed that $\Delta\phi/\phi_0$ saturates at high electric field strengths ($E_n \geq 3.25$ kV/cm). These results are reminiscent of bubbling stimulation in vibrofluidized beds at high vibration intensities in the range of small vibration frequencies.[30] In fact, a commonality between these types of enhanced fluidization techniques is that in both cases the excitations are predominantly concentrated at the bottom of the bed.

The unsieved nanopowder has a rather polydisperse agglomerate size distribution ranging from $\sim$10 μm to some sizes on the order of 1 mm. Thus, before all the above reported experiments, the R974 silica nanopowder had to be presieved to remove agglomerates larger than 425 μm that impeded proper initialization. Previous sample sieving has been systematically used in assisted fluidization techniques. The removal of these large and hard agglomerates helps the average sized agglomerates fluidize. The particularly interesting field distribution caused by the variable electric field configuration in our experiment led us to study the effect of this assisted fluidization technique on the fluidization behavior of unsieved nanopowder.

The first experiment consisted of conventionally fluidizing (without any external excitations) the unsieved nanopowder. The bed expansion was found to be quite poor as expected due to the inability of the larger agglomerates to fluidize. These larger agglomerates sink to the bottom of the bed and hinder a uniform distribution of the gas flow within the bed thus favoring gas channeling. Once the electric field was turned on ($f = 20$ Hz, $E_n = 4$ kV/cm), it was seen however that the bed began to expand immediately. Then, the nanopowder was allowed to fluidize once more conventionally after the electric field was turned off in order to see if the enhanced fluidization effect of the field was irreversible.

Figure 14 shows the relative variation of the particle volume fraction (with respect to the packed state) as a function of superficial gas velocity according to this procedure. In this figure, it can be seen that the application of the nonuniform electric field has a remarkable effect on the expansion behavior of the unsieved nanopowder, which fluidized

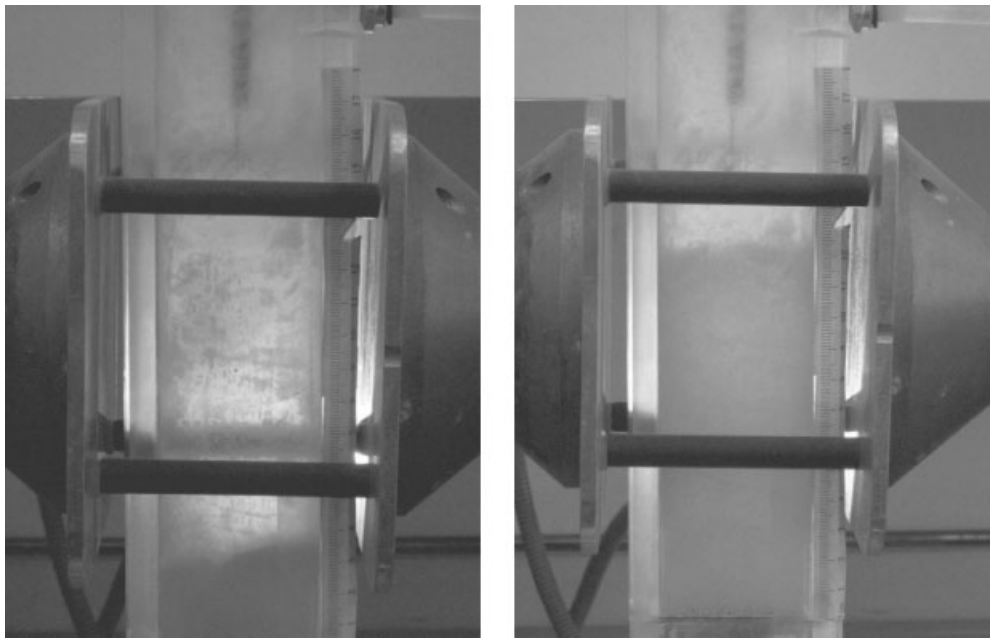

Figure 15. Snapshots of a fluidized bed of unsieved R974 silica before (left) and after (right) the electric field was applied (variable field configuration).

heterogeneously in the absence of external field with rather small expansion. Relative increments on bed expansion of almost 80% were obtainable when the field was applied. Data from conventional fluidization of presieved silica is shown for comparison. As can be observed, the level of expansion obtained by application of the alternating nonuniform field to the unsieved fluidized bed of silica is comparable to the expansion observed for the conventional poorly fluidized bed of presieved silica. Figure 15 shows a photograph of the unsieved nanopowder fluidized at the maximum gas velocity ($u_g \approx 3$ cm/s) before and after the electric field was applied. This figure clearly illustrates that the application of the nonuniform alternating electric field has a dramatic effect on the fluidization expansion of the unsieved nanopowder. It is observed, however, that the bigger agglomerates remain still deposited at the bottom of the bed, indicating that, though the electric field produces strong agitation of these agglomerates, it does not break them, though it facilitates a uniform distribution of the gas flow to the rest of the bed. Thus, when the field is turned off, the fluidization state of the unsieved silica returns to its heterogeneous state as can be seen in Figure 14.

Conclusions

A number of techniques have been proposed in the literature to enhance the fluidization quality of nanopowders such as external vibration, sound wave pulsation, centrifugation, and addition of large magnetic particles that are excited by a variable magnetic field. These techniques have been shown to serve to enhance expansion of fluidized beds of silica nanopowders, which were sieved before fluidization. In this article, we demonstrate that the application of either a cross-flow or a co-flow alternating electric field is also useful to enhance fluidization of this system. However, the most effective technique to assist fluidization has been shown to consist of application of a nonuniform alternating electric field, which is weak in the vicinity of the free surface but strong close to the bottom of the bed. Because of the wide size distribution of the nanoparticle agglomerates, especially in the case of unsieved samples ranging from 10 of microns to millimeters, the conventional fluidized bed is highly stratified, with the larger agglomerates sinking to the bottom of the bed and the smaller agglomerates almost in suspension close to the free surface. These smaller agglomerates are easily elutriated if the gas flow is increased to mobilize the larger agglomerates or other assisted fluidization techniques are used. It has been shown in this work that the alternating nonuniform field strongly agitates the larger agglomerates, which destabilizes the development of gas channels close to the distributor thus enhancing fluidization. Furthermore, the variable field has almost no effect on the smaller agglomerates at the top of the bed, thus avoiding excessive elutriation. By using this technique, the nanopowder does not have to undergo a pretreating sieving process, which has been critical to most fluidization studies of R974 silica. It is remarkable that the action of the field is noticeable without the need of electrostatically precharging the nanopowder. Because of contact and tribo charging mechanisms, the nanoparticle agglomerates naturally accumulate sufficient electrostatic charge to be appreciably excited by electrostatic fields of strength on the order of 1 kV/cm. Nevertheless, in this work, we have carried out tests on artificially precharged nanopowder samples by means of corona discharge. This technique has been found to be counterproductive in further enhancing fluidization, which is mainly due to nanopowder sticking to the metallic distributor plate.

Acknowledgments

The authors would like to thank the invaluable assistance of Dr. Miguel Angel Sanchez Quintinilla for the preparation of the experimental setup and simulations. Professors Antonio Castellanos and Alberto T. Perez are also acknowledged for fruitful discussions concerning corona discharge results. The Seville group acknowledges the Spanish Government Agency Ministerio de Ciencia y Tecnologia (contract FIS2006-03645) and Junta de Andalucia (contract FQM 421). The NJIT group acknowledges support from the National Science Foundation through Grant DMI 0210400, NIRT: Collaborative Research: Experimental and Computational Investigations of Fluid Interactions/Transport in Nanodomains and Around Nanoparticles. The NJIT group would also like to acknowledge support from the National Science Foundation through Grant DGE 0504497, IGERT in Nano Pharmaceutical Engineering, and through an IREE Grant (DMI 0506722). Both groups wish to thank Dr. Herbert Riemenschneider and the Degussa Company for supplying the nanoparticles used in the experiments.

Literature Cited

1. Geldart D. Types of gas fluidization. *Powder Technol.* 1973;7:285–293.
2. Rietema K. *The Dynamics of Fine Powders*. London: Elsevier, 1991.
3. Jackson R. *The Dynamics of Fluidized Particles*. Cambridge: Cambridge University Press, 2000.
4. Tsinontides SC, Jackson R. The mechanics of gas-fluidized beds with an interval of fluidization. *J Fluid Mech.* 1993;255:237–274.
5. Menon N, Durian DJ. Particle motions in a gas-fluidized bed of sand. *Phys Rev Lett*. 1997;79:3407–3410.
6. Seville JPK, Clift RC. The effect of thin liquid layers on fluidization characteristics. *Powder Technol.* 1984;37:117–129.
7. Xie H-Y, Geldart D. Fluidization of FCC powders in the bubble-free regime: effect types of gases and temperature. *Powder Technol.* 1995;82:269–277.
8. Colver GM. An interparticle force model for ac-dc electric fields in powders. *Powder Technol.* 2000;112:126–136.
9. Johnson TW, Melcher JR. Electromechanics of electrofluidized beds. *Ind Eng Chem Fundam.* 1975;14:146–153.
10. van Willigen FK, van Ommen JR, van Turnhout J, van den Bleek CM. Bubble size reduction in electric-field-enhanced fluidized beds, *J Electrostat.* 2005;63:943–948.
11. Glor M. *Electrostatic Hazards in Nanopowder Handling*. New York: Wiley, 1988:425–440.
12. Valverde JM, Ramos A, Castellanos A, Watson PK. The tensile strength of cohesive powders and its relationship to consolidation, free volume and cohesivity. *Powder Technol.* 1998;97:237–245.
13. Quintanilla MAS, Valverde JM, Castellanos A. Adhesion force between fine particles with controlled surface properties. *AIChE J.* 2006;52:1715–1728.
14. Chen Y, Yang J, Dave RN, Pfeffer R. Fluidization of Coated Group C Powders. *AIChE J*. 2008;54:104–121.
15. Valverde JM, Castellanos A, Quintanilla MAS. Self-diffusion in a gas-fluidized bed of fine nanopowder. *Phys Rev Lett.* 2001;86: 3020–3023.
16. Castellanos A, Valverde JM, Quintanilla MAS. Aggregation and sedimentation in gas-fluidized beds of cohesive powders. *Phys Rev E*. 2001;64:1–7.
17. Valverde JM, Castellanos A. Types of gas fluidization of cohesive granular materials. *Phys Rev E*. 2007;75:031306.
18. Valverde JM, Quintanilla MAS, Castellanos A, Lepek D, Quevedo J, Dave RN, Pfeffer R. Fluidization of fine and ultrafine particles using nitrogen and neon as fluidizing gases. *AIChE J*. 2008;54:86–103.

19. Chaouki J, Chavarie C, Klvana D, Pajonk G. Effect of Interparticle forces on the hydrodynamic behavior of fluidized aerogels. *Powder Technol.* 1985;43:117–125.
20. Chavarie C, Dobson K, Clift R, Seville JPK. *Proceedings of 37th Canadian Chemical Engineering Conference,* Montreal, Ottawa, May 1987, p 216.
21. Morooka S, Kusakabe K, Kobata A, Kato Y. Fluidization state of ultrafine powders. *J Chem Eng Jpn.* 1988;21:41–46.
22. Brooks EF, Fitzgerald TJ. Fluidization of novel tendrillar carbonaceous materials. In: Ostergaard K, Sorensen A, editors. *Fluidization.* New York: Engineering Foundation, 1986:217–224.
23. Li H, Legros R, Brereton CMH, Grace JR, Chaouki J. Hydrodynamic behaviour of aerogel powders in high-velocity fluidized beds. *Powder Technol.* 1990;60:121–129.
24. Pacek AW, Nienow AW. Fluidisation of fine and very dense hard-metal powders. *Powder Technol.* 1990;60:145–158.
25. Zhu C, Yu Q, Dave RN, Pfeffer R. Gas fluidization characteristics of nanoparticle agglomerates. *AIChE J.* 2005;51:426–439.
26. Nam C, Pfeffer R, Dave RN, Sundaresan S. Aerated vibrofluidization of silica nanoparticles. *AIChE J.* 2004;50:1776–1785.
27. Wang XS, Palero V, Soria J, Rhodes MJ. Laser-based planar imaging of nano-particle fluidization: Part I—determination of aggregate size and shape. *Chem Eng Sci.* 2006;61:5476–5486.
28. Yao W, Guangsheng G, Fei W, Wu J. Fluidization and agglomerate structure of SiO_2 nanoparticles. *Powder Technol.* 2002; 124:152–159.
29. Valverde JM, Castellanos A. Fluidization of nanoparticles: a modified Richardson-Zaki law. *AIChE J.* 2006;52:838–842.
30. Quintanilla MAS, Valverde JM, Castellanos A, Lepek D, Pfeffer R, Dave RN. Nanofluidization as affected by vibration and electrostatic fields. *Chem Eng Sci.* 2008;63:5559–5569.
31. Zhu C, Liu G, Yu Q, Pfeffer R, Dave RN, Nam C. Sound assisted fluidization of nanoparticle agglomerates. *Powder Technol.* 2004; 141:119–123.
32. Quevedo J, Pfeffer R, Shen Y, Dave R, Nakamura H, Watano S. Fluidization of nanoagglomerates in a rotating fluidized bed. *AIChE J.* 2006;52:2401–2412.
33. Yu Q, Dave RN, Zhu C, Quevedo JA, Pfeffer R. Enhanced fluidization of nanoparticles in an oscillating magnetic field. *AIChE J.* 2005;51:1971–1979.
34. Valverde JM, Quintanilla MAS, Espin MJ, Castellanos A. Nanofluidization electrostatics. *Phys Rev E.* 2008;77:031301.
35. Kashyap M, Gidaspow D, Driscoll M. Effect of electric field on the hydrodynamics of fluidized nanoparticles. *Powder Technol.* 2008; 183:441–453.
36. Valverde JM, Quintanilla MAS, Espin MJ, Castellanos A. Fluidizacion de polvos finos y ultrafinos asistida por campos electricos oscilantes. Patent P200802055, Asignee: University of Seville, July 10, 2008.
37. Valverde JM, Castellanos A, Quintanilla MAS. The memory of granular materials. *Contemp Phys.* 2003;44:389–399.
38. Bendaoud B, Dascalescu L, Blajan M, Samuila A, Stochita A, Notingher PV. Corona charging of granular layers of insulating particles at the surface of a grounded electrode. *J Electrostat.* 2005; 63:643–647.
39. Rickard M, Dunn-Rankin D, Weinberg F, Carleton F. Characterization of ionic wind velocity. *J Electrostat.* 2005;63:711–716.
40. Lipowicz PJ, Yeh HC. Fiber dielectrophoresis. *Aerosol Sci Technol.* 1989;11:206–212.
41. Pohl HA. Nonuniform field effects: dielectrophoresis. In: Moore AD, editor. *Electrostatics and Its Applications.* New York: Wiley, 1973:336–362.
42. http://www.matweb.com.

Appendix

Evaluation of the dielectrophoretic force

The total electric force acting on a suspended particle of net charge Q in a non-uniform field $\mathbf{E}$ is given by

$$\mathbf{F} = Q\mathbf{E} + (\mathbf{p} \cdot \nabla)\mathbf{E}. \tag{A1}$$

where Q is the net charge on the particle, $\mathbf{p}$ is the dipole moment of the particle, and $\mathbf{E}$ is the electric field vector. The second term in the right-hand side of Eq. A1, involving the dipole moment and field gradient, is known as dielectrophoretic force, arising from the polarization of matter and its subsequent tendency to move into regions of diverging field intensity. For charged particles in a electrostatic field, the first term in the right-hand side of Eq. A1, involving the direct attraction of the electric field for a charge (electrophoresis) is dominant. Because it is practically impossible to have uncharged particles in a nanopowder sample,[34] the electrophoretic influence is usually dominant, though it can be nullified by using a high frequency alternating field instead of a static field.[40]

Dielectric particles placed in an electric field become polarized according to their electrical permittivity and thus experience a dielectrophoretic force if the field is not uniform. For a sphere of diameter d_p, this force is approximately given by[41]

$$F_d \simeq \frac{\pi d_p^3}{12} \varepsilon_1 \frac{\varepsilon_2 - \varepsilon_1}{\varepsilon_2 + 2\varepsilon_1} \nabla E^2 \tag{A2}$$

where E is the strength of the electric field applied, and ε_1 and ε_2 are the permittivities of the surrounding fluid and sphere, respectively. In general, dielectrophoresis is an effect requiring quite divergent fields and usually requires sizable differences in the permittivities of the particle and the surrounding medium.[41] In our experiments, we have a maximum value of $\nabla E^2 \backsimeq 0.4 \times 10^{12} \mathrm{V}^2/\mathrm{cm}^3$ for the variable field configuration. If we consider silica agglomerates as effective particles of maximum size $d_p \backsimeq 1$ mm, and using $\varepsilon_0 = 8.854 \times 10^{-12}$ F/m, $\varepsilon_2 = 1.14\varepsilon_0$ (value reported for silica aerogel[42]), we have a maximum dielectrophoretic force $F_d \backsimeq 0.04$ nN according to Eq. A2, which is negligible when compared with agglomerate weight. Dielectrophoresis does not play, therefore, a role in our system, though it should be taken into account in variable field configurations; specially, when high permittivity materials are used.

Manuscript received Dec. 5, 2008, and revision received Apr. 20, 2009.